Dark Space ahead of a Shock in Ionized Gas Flows

Michio Nishida
Department of Aeronautical Engineering, Kyoto University, Kyoto, Japan

Z. Naturforsch. **36 a**, 980–991 (1981); received May 27, 1981

The dark space, which is formed ahead of a detached shock of a blunt body in a flow of ionized argon, was theoretically investigated, and its mechanism was revealed. The electron energy equation, electron continuity equation and continuity equation of the first excited-level atoms were formulized separatly in a shock layer and in a free stream, and then the free-stream solutions were connected with the shock-layer solutions in such a way that the boundary conditions on the wall of the blunt body are satisfied. The method of solving is described here. The calculations were carried out for the case that atom density is 10^{21} particles/m^3, atom temperature is 500 K, Mach number is 4.5, electron density is 5×10^{18} particles/m^3 in the free stream and that the wall temperature is 300 K. The results show that the region of the elevated electron temperature exists ahead of the shock and that this elevation causes the decrease in the population densities of excited levels higher than the 5s level. The dark space can be explained as the reduction in the population densities due to the elevation in the electron temperature.

I. Introduction

There exists a region ahead of a detached shock of a blunt body in an ionized-gas flow where the self-luminosity of a flow is reduced (cf. Figure 1). This region is called "dark space" and is observed not only ahead of the detached shock of the blunt body but also ahead of a Mach disk in ionized free-jet expansions. The dark space is associated with the variation of electron temperature in front of the shock. According to Grewal and Talbot [1], the dark space results from the elevated electron temperature ahead of the shock. Namely, there exists a broad zone of elevated electron temperature ahead of the electron compression region, caused by the high thermal-conductivity in the electron gas. When the electron density remains unchanged in this region, the elevated electron temperature reduces the recombination rate. Since the self-luminosity of the flow is due to the recombination radiation, the dark space is observed in the region of elevated electron temperature. Since this explanation is in complete, detailed investigations of the behaviour of radiation-emitting atoms, i.e. electronically excited atoms, are required to reveal the dark space phenomenon.

Our interert here is in exploring the formation of the dark space that appears ahead of the detached shock of a blunt body placed in the flow of partially ionized argon gas. Under the conditions where this problem is considered, the gas is rarefied and hence the region between the detached shock and the body is considered as a viscous shock layer. Also, three nonequilibrium states are observed in the present case. One is the thermal nonequilibrium, that is the temperature differences between electrons and heavy particles. A second nonequilibrium is the ionizational nonequilibrium. A third non-

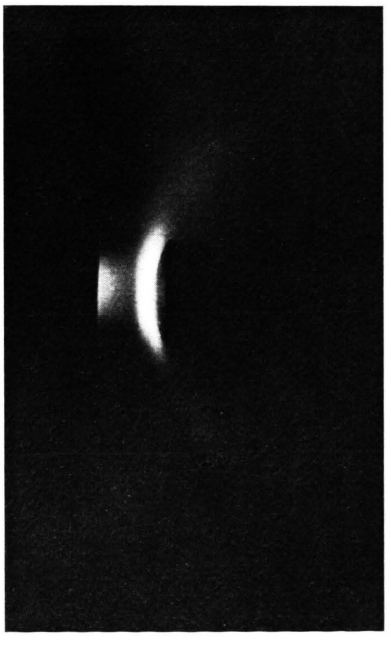

Fig. 1. Dark Space ahead of a Detached Shock of a Blunt Body.

Reprint requests to Prof. M. Nishida, Department of Aeronautical Engineering, Kyoto University, Kyoto/Japan.

0340-4811 / 81 / 0900-0980 $ 01.00/0. — Please order a reprint rather than making your own copy.

equilibrium is the electronical nonequilibrium, which is such that electronically excited levels are not populated according to the Boltzmann-equilibrium relation. In a laboratory experiment such as an arc-heated low-density plasma, these three nonequilibrium states simultaneously exist. Therefore we must include these nonequilibrium phenomena into the present analysis by formulating the continuity equations of the electrons and the excited atoms, and the electron energy equation. The formulations were made separately in the free stream and in the shock layer, and by using the jump relation across the shock, the two solutions in the free stream and in the shock layer are connected. Electronically excited-atoms densities on a stagnation stream line are numerically calculated, and based on the result of the excited-atom density profiles, the dark space will be discussed.

Since the simple explanation of the dark space made by Grewal and Talbot there have been no satisfactory explanations. Christiansen [2] measured the radiation intensity upstream of the shock caused by a blunt body, but he did not discuss the number density of the bound electronic-levels from which the radiation originated.

II. Formulation in Shock Layer

A) Basic Equations

The following assumptions are introduced: 1) The gas is composed of argon atoms, ions and electrons; 2) the degree of ionization $\alpha_e \ll 1$; 3) there are no external magnetic and electric fields; 4) the atoms and ions have essentially the same average velocity because of their almost equal mass; 5) there is ambipolar diffusion; 6) charge neutrality is established so that the electrons and heavy particles have the same average velocity; 7) the atom temperature is equal to the ion temperature; 8) the sheath thickness is negligible compared with the shock-layer thickness; and 9) a collision-free sheath is considered. The atoms also are divided into those in electronically excited levels, and it may be considered that the number density of the atoms in the ground level is much larger than that in any other level. On the other hand, since the degree of ionization is negligible compared with unity, the over-all flow is not influenced by the existence of the charged particles. Hence the flow is dominated by the atoms in the ground level. Thus, the over-all continuity, momentum, and energy equations of the gas of interest are essentially those of the atoms in the ground level.

The shock layer considered is a partially ionized, viscous shock layer in front of a blunt body which is at floating potential. We treat the case where the Rankine-Hugoniot condition across the shock is satisfied. However, the number density of the atoms in any excited level higher than the 4s level does not obey the Rankine-Hugoniot relation because the relaxation time of such a level is much smaller than the characteristic flow time as mentioned later. Also, there is no jump across the shock in the electron temperature, while it exists in the heavy-particle temperature [1, 3].

As mentioned before, the over-all shock layer equations are not coupled with those of the electrons and the excited atoms so that the over-all equations are independently analyzed. Based on the assumptions 4), 6) and 7), the equations to be solved here are the continuity equations of the excited atoms and the electrons, and the energy conservation equation of the electrons. First of all, we consider the basic equations of the excited atoms. The energy level structure of the neutral argon atoms used here is summarized in Table 1. All the levels above level 9s are assumed to be in equilibrium with the free electrons so that the excited-atom densities of such levels can be determined by the Saha-equilibrium relation. Under the present conditions, the characteristic flow time of a gas through the shock layer is of the order of 10^{-5} s, while the relaxation time of the excited levels above level 4s is of an order less than 10^{-8} s. A steady state assumption may, therefore, be made for the

Table 1. Energy Level Model of Neutral Argon.

j	Term	$g(j)$	j	Term	$g(j)$
1	$3p^6$	1	12	7s	12
2	$3p^5 4s$	12	13	5f	84
3	4p	36	14	7p	36
4	3d	60	15	6d	60
5	5s	12	16	8s	12
6	5p	36	17	6f	84
7	4d	60	18	8p	36
8	6s	12	19	7d	60
9	4f	84	20	9s	12
10	6p	36	21	8d	40
11	5d	60			

levels from level 4p to level 9s, which leads to the equation

$$\dot{n}(j) = 0\,, \quad j = 3, 4, 5, \ldots, 20\,, \tag{1}$$

where $\dot{n}(j)$ is the net production rate of the population density of level j [4]. On the other hand, the relaxation time of level 4s is in the range from 10^{-6} s to 10^{-4} s under the assumption that, as a first approximation, the radiation originating from level 4s is trapped, so that the steady state assumption does not hold for this level. Using the coordinate system as shown in Fig. 2, where u and v are the velocities in the x- and y-directions, respectively, and U_∞ is the free-stream velocity, we can write the continuity of the excited atoms in level 4s as follows:

$$\varrho\, u \frac{\partial \alpha_2}{\partial x} + \varrho\, v \frac{\partial \alpha_2}{\partial y} = m_a \dot{n}(2)\,, \tag{2}$$

with

$$\alpha_2 = n(2)/n\,, \quad n = \sum_{j=1}^{\infty} n(j) + n_e \cong n(1)\,, \tag{3}$$

$$\varrho = m_a \sum_{j=1}^{\infty} n(j) + m_i n_i + m_e n_e \cong m_a n(1)\,,$$

where $n(j)$ is the population density of level j, n_k the number density of species k, m_k the mass of species k, ϱ the mass density, and the subscripts a, i and e refer to the atoms, ions and electrons, respectively.

The continuity and energy equations of the electrons are given by

$$\varrho\, u \frac{\partial \alpha_e}{\partial x} + \varrho\, v \frac{\partial \alpha_e}{\partial y} + \frac{\partial}{\partial y}(\varrho_i V_d) = m_i \dot{n}_e\,, \tag{4}$$

$$\varrho\, u \frac{\partial}{\partial x}(\alpha_e C_p T_e) + \varrho\, v \frac{\partial}{\partial y}(\alpha_e C_p T_e) = u \frac{\partial p_e}{\partial x} + (v + V_d) \frac{\partial p_e}{\partial y} + \frac{\partial}{\partial y}\left(\lambda_e \frac{\partial T_e}{\partial y}\right) - \frac{\partial}{\partial y}(C_p \varrho_i V_d) + R + L \tag{5}$$

with

$$\alpha_e = n_e/n\,, \quad \varrho_i = m_i n_e\,,$$
$$C_p = (5/2)\, k_B/m_a\,, \quad p_e = n_e k_B T_e\,. \tag{6}$$

In (4) and (5), V_d is the diffusion velocity, T_e the electron temperature, λ_e the thermal conductivity of the electrons, R the electron-energy transfer rate due to elastic collisions, L the electron-energy transfer rate due to inelastic collisions, $\dot{n}_e$ the net production rate of the electrons and k_B the Boltzmann constant.

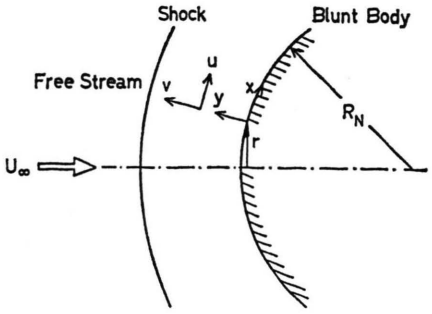

Fig. 2. Coordinate System.

The net production rate of the population density of level j is given by

$$\begin{aligned}\dot{n}(j) = &\sum_{s=1}^{\infty} [Q(s,j)\, n_e\, n(s) - Q(j,s)\, n_e\, n(j)] \\ &+ Q_R(\infty, j)\, n_e{}^2 - Q_I(j, \infty)\, n_e\, n(j) \\ &+ \sum_{s=j+1}^{\infty} \beta(s,j)\, A(s,j)\, n(s) \\ &- \sum_{s=1}^{j-1} \beta(j,s)\, A(j,s)\, n(j) \\ &+ \beta(\infty, j)\, A(\infty, j)\, n_e{}^2\,,\end{aligned} \tag{7}$$

where $Q(s,j)$ is the rate constant for an electron-collisional transition from level s to level j, $Q_R(\infty, j)$ the collisional recombination rate-constant to level j, $Q_I(j, \infty)$ the collisional ionization rate-constant from level j, $A(s,j)$ the Einstein A coefficient for a radiative transition from level s to level j, $A(\infty, j)$ the radiative recombination rate-constant to level j and $\beta(j,s)$ the radiative-escape factor. In the order in which they appear, the terms on the right hand side of (7) represent the following contribution to the population of the level j: electron-collisional excitation and de-excitation from any level to the level j, electron-collisional excitation and de-excitation from the level j to any level, collisional recombination to the level j, collisional ionization from the level j, radiative transitions from any upper level to the level j, radiative transitions from the level j to any level, and radiative recombination to the level j. Atom-collisional transitions are insignificant compared with electron-collisional transitions in the range of the atom temperature considered here.

Now, we express the net production rate of the electrons in terms of population density and col-

lisional-ionization rate constant. Radiative recombination can be neglected compared with collisional recombination, under the present conditions. Using the principle of detailed balancing, we get

$$\dot{n}_e = n_e \sum_{j=1}^{\infty} [Q_I(j,\infty)\{n(j) - n_{eq}(j)\}], \tag{8}$$

where $n_{eq}(j)$ is the equilibrium population density of level j from the Saha equilibrium relation.

The electron energy transfer rate due to the inelastic collisions, L, includes those due to electron-collisional transitions between bound levels, due to the collisional ionization-recombination and also due to the radiative recombination. It is written, for $k>j$, as

$$\begin{aligned} L = &- \sum_{k=2}^{\infty} \sum_{j=1}^{k-1} (E_k - E_j) \\ &\cdot [Q(j,k)\, n_e\, n(j) - Q(k,j)\, n_e\, n(k)] \\ &- n_e \sum_{j=1}^{\infty} (E_I - E_j)[n(j) - n_{eq}(j)]\, Q_I(j,\infty) \\ &- \tfrac{3}{2} k_B T_e n_e^2 \sum_{j=1}^{\infty} \beta(\infty,j)\, A(\infty,j), \end{aligned} \tag{9}$$

where E_k is the excitation energy measured from the ground level and E_I the ionization energy from the ground level. By multiplying (7) by $(E_I - E_j)$, summing over all j and then using the resultant equation in (9), we have

$$L = \sum_{j=1}^{\infty} (E_I - E_j)\, \dot{n}(j) + L_{rad} \tag{10}$$

with

$$\begin{aligned} L_{rad} = &- \sum_{k=2}^{\infty} \sum_{j=1}^{k-1} \beta(k,j)\, A(k,j)\, n(k)(E_k - E_j) \\ &- \sum_{k=1}^{\infty} \beta(\infty,k)\, A(\infty,k) \\ &\cdot n_e^2 [E_I - E_k + (3/2)\, k_B T_e]. \end{aligned} \tag{11}$$

Since we have assumed $\dot{n}(j) = 0$ for $j \geqq 3$, (10) can be rewritten as

$$L = \dot{n}(1) + \dot{n}(2)(E_I - E_2) + L_{rad}. \tag{12}$$

The electron energy transfer rate due to the elastic collisions, R, is expressed as [5]

$$R = 2\, n_e m_e \sum_{k=a,i} \{\bar{\nu}_{ek}/m_k [(3/2)\, k_B (T_k - T_e)]\}, \tag{13}$$

where $\bar{\nu}_{ek}$ represents the collision frequency for the electron-k-species encounters and T_k the temperature of the species k. Using the Coulomb cross section for the electron-ion encounters, the average electron-ion collision frequency is of the form [6]

$$\bar{\nu}_{ei} = \frac{8}{3} \left(\frac{\pi}{m_e}\right)^{1/2} \frac{n_e e^4}{(2 k_B T_e)^{3/2}} \ln\left(\frac{9 k_B^3 T_e^3}{4\pi n_e e^6}\right), \tag{14}$$

where e is the electronic charge. The average collision frequency is expressed as [7]

$$\bar{\nu}_{ea} = n_a (8 k_B T_e/\pi m_e)^{1/2}\, \sigma_{ea}(T_e). \tag{15}$$

For the argon atoms, σ_{ea} is approximately expressed as [8]

$$\begin{aligned} \sigma_{ea} &= (0.39 - 0.551 \times 10^{-4} T_e + 0.595 \times 10^{-8} T_e^2) \\ &\quad \times 10^{-20} m^2 \quad \text{for} \quad T_e < 10^4\ \mathrm{K}, \\ \sigma_{ea} &= (-0.35 + 0.775 \times 10^{-4} T_e) \\ &\quad \times 10^{-20} m^2 \quad \text{for} \quad T_e \geqq 10^4\ \mathrm{K}. \end{aligned} \tag{16}$$

According to the work of Jaffrin [3], the thermal conductivity of the electrons is written as

$$\lambda_e = \frac{75\, k_B}{64\sqrt{2}} \left(\frac{\pi k_B T_e}{m_e}\right)^{1/2} \frac{n_e}{n_a \sigma_{ea} + (1+\sqrt{2})\, n_e \sigma_{ee}}, \tag{17}$$

where σ_{ee} is the Coulomb cross section. Since the sheath thickness is negligible compared with the shock layer thickness, we may consider that diffusion of charged particles is ambipolar. For a two-temperature plasma, the ambipolar diffusion velocity is given by [9]

$$V_d = - \frac{D_a}{\alpha_e} \left[\frac{\partial \alpha_e}{\partial y} + \frac{\alpha_e (1-\alpha_e)}{1+\tilde{\Omega}} \frac{\partial \tilde{\Omega}}{\partial y}\right], \tag{18}$$

where $\tilde{\Omega} = T_e/T_a$ and D_a is the ambipolar diffusion coefficient defined by

$$D_a = \frac{\bar{\mu}_e + \bar{\mu}_i}{\bar{\mu}_e \bar{\mu}_i} \frac{k_B T_a}{e} \frac{1+\tilde{\Omega}}{1+\alpha_e \tilde{\Omega}}, \tag{19}$$

in which $\bar{\mu}$ and $\bar{\mu}_i$ are the mobilities of the electrons and ions, respectively. Using the relations $\bar{\mu}_e \gg \bar{\mu}_i$ and $\bar{\mu}_i \cong e/m_i \bar{\nu}_{ia}$, (19) becomes

$$D_a = \frac{k_B T_a}{m_i \bar{\nu}_{ia}} \frac{1+\tilde{\Omega}}{1+\alpha_e \tilde{\Omega}}, \tag{20}$$

where

$$\bar{\nu}_{ia} = n_a (8 k_B T_i/\pi m_i)^{1/2}\, \sigma_{ia}, \tag{21}$$

$$\sigma_{ia} = 1.4 \times 10^{-18} m^2. \tag{22}$$

B) Boundary Conditions

When a body which is electronically insulated or to which an electric field is not applied, is placed in

the ionized gas, it will be at floating potential, and the ion sheath will be produced on the wall of the body. In this case, since the body draws no currents, the net currents normal to the wall vanish. Using the condition of no normal net-currents, the continuity conditions at the sheath edge for fluxes of electron energy and ion mass lead to the following boundary conditions at the wall [10]:

$$(\partial\alpha_e/\partial y)_w = (k_B T_{e_w}/m_a)^{1/2}\alpha_{e_w}/D_{a_w}, \tag{23}$$

$$(\partial T_e/\partial y)_w = -(1/2)[1+\ln(2\pi)+\ln\varepsilon] \cdot n_{e_w}(k_B T_{e_w})^{3/2}/\lambda_{e_w} m_a^{1/2}, \tag{24}$$

where $\varepsilon = m_e/m_a$ and the subscript w denotes the wall condition. The boundary condition at the edge of the shock layer are

$$[\alpha_2]_{y=y_s} = \alpha_{2_s} = \alpha_{2_u}, \tag{25}$$

$$[\alpha_e]_{y=y_s} = \alpha_{e_s} = \alpha_{e_u}, \tag{26}$$

where the subscripts s and u denote the edge of the shock layer and the position immediately ahead of the shock, respectively. The boundary condition for the electron temperature is determined from the free-stream solution. The method to solve the electron energy equation in the shock layer is described later.

C) Coordinate Transformation

In order to obtain similar solutions near the stagnation stream line, the following transformation of coordinate is employed:

$$\xi(x) = \int_0^x (\varrho\mu)_s u_s r^{2j}\,dx,$$

$$\eta(x,y) = u_s r^{2j}/(2\xi)^{1/2}\int_0^y \varrho\,dy, \tag{27}$$

where $j=0$ and $j=1$ represent a two-dimensional flow and an axisymetric flow, respectively, and μ is the viscosity. In addition, the following dimensionless quantities are introduced:

$$V = \frac{2\xi}{(\varrho\mu)_s u_s r^{2j}}\left[f'\frac{\partial\eta}{\partial x} + \frac{\varrho v r^j}{(2\xi)^{1/2}}\right],$$

$$f' = u/u_s, \quad \theta = T_a/T_{a_s}, \quad \Theta = T_e/T_{a\infty},$$

$$z_e = \alpha_e/\alpha_{e_s}, \quad z_2 = \alpha_2/\alpha_{2_s}, \quad \Omega = \Theta/\theta, \tag{28}$$

where the subscript ∞ denotes the free-stream condition. The electron temperature is non-dimensionalized by the atom temperature in the free stream for future convenience. Using (27) and (28), (2), (4) and (5) are, near the stagnation stream line, transformed to

$$dz_2/d\eta = (\tau_u/\alpha_{2_s} n_s)(\theta/V)\dot{n}(2), \tag{29}$$

$$\frac{d}{d\eta}\left(\frac{l}{Sc}\frac{dz_e}{d\eta}\right) + \frac{d}{d\eta}\left[\frac{l}{Sc}\frac{\tau(1-\alpha_{e_s}z_e)}{1+\tau\Omega}\frac{d\Omega}{d\eta}\right] - V\frac{dz_e}{d\eta} = -\frac{\alpha_u}{\alpha_{e_s} n_s}\theta\dot{n}_e, \tag{30}$$

$$F_1 d^2\Theta/d\eta^2 + F_2 d\Theta/d\eta + F_3\Theta + F_4 = 0, \tag{31}$$

with

$$F_1 = l/Pr_e,$$

$$F_2 = \frac{d}{d\eta}\left(\frac{l}{Pr_e}\right) - \frac{3}{5}\alpha_{e_s} V z_e + \frac{3}{5}\frac{l}{Sc} \cdot\left\{\frac{dz_e}{d\eta} + \frac{\tau z_e(1-\alpha_{e_s}z_e)}{1+\tau\Omega}\frac{d\Omega}{d\eta}\right\}\alpha_{e_s},$$

$$F_3 = \alpha_{e_s}\frac{d}{d\eta}\left\{\frac{l}{Sc}\frac{dz_e}{d\eta} + \frac{l}{Sc}\frac{\tau z_e(1-\alpha_{e_s}z_e)}{1+\tau\Omega}\frac{d\Omega}{d\eta}\right\} - \alpha_{e_s} V\frac{dz_e}{d\eta} + \frac{2}{5}\frac{\alpha_{e_s}}{\psi} \cdot\left\{V - \frac{l}{Sc}\frac{1}{z_e}\frac{dz_e}{d\eta} - \frac{l}{Sc}\frac{\tau(1-\alpha_{e_s}z_e)}{1+\tau\Omega}\frac{d\Omega}{d\eta}\right\} \cdot\frac{d}{d\eta}(z_e\psi),$$

$$F_4 = \frac{\tau_u}{C_p T_{a\infty}\varrho_s}\theta(R+L),$$

$$\tau_u = 2\xi/(\varrho\mu)_s u_s^2 r^{2j}, \quad \psi = n_e/n_{e_s} = z_e/\theta,$$

$$l = \varrho\mu/(\varrho\mu)_s, \quad Pr_e = \mu C_p/\lambda_e,$$

$$Sc = \mu/\varrho D_a, \quad \tau = T_{a\infty}/T_{a_s}. \tag{32}$$

Using the relation $\mu = (5\pi/32)(8k_B T_a/\pi m_a)/\sigma_{aa}$, the ambipolar Schmidt number, Sc, is written as

$$Sc = \frac{5}{4}\frac{\sigma_{ia}}{\sigma_{aa}}\frac{(1-\alpha_{e_s}z_e)(1+\tau\alpha_{e_s}z_e\Omega)}{1+\tau\Omega}, \tag{33}$$

where σ_{aa} is given by [11]

$$\sigma_{aa} = 1.70\times10^{-18} T_a^{-1/4} m^2. \tag{34}$$

Near the stagnation stream line, $r=x$ and $u_s = u_{1s}x$, where $u_{1s} = U_\infty/R_N$, so that τ_u is rewritten as $\tau_u = 1/[(1+j)u_{1s}]$.

The boundary conditions (23) and (24) are transformed to

$$\left(\frac{dz_e}{d\eta}\right)_w = \left[\frac{1}{1+j}\frac{(\varrho\mu)_s}{u_{1s}}\right]^{1/2} \cdot \frac{Sc_w}{\mu_w}\left(\frac{k_B T_{a\infty}}{m_a}\right)^{1/2} \Theta_w^{1/2} z_{e_w} - \frac{\tau z_{e_w}(1-\alpha_{e_s} z_{e_w})}{1+\tau\Theta_w/\theta_w} \cdot \left[\frac{1}{\theta_w}\left(\frac{d\Theta}{d\eta}\right)_w - \frac{\Theta_w}{\theta_w^2}\left(\frac{d\theta}{d\eta}\right)_w\right], \quad (35)$$

$$\left(\frac{d\Theta}{d\eta}\right)_w = -\frac{1+\ln(2\pi\varepsilon)}{2(1+j)}\frac{(\varrho\mu)_s \alpha_{e_s}}{u_{1s}} \cdot \left(\frac{k_B^3 T_{a\infty}}{m_a^3}\right)^{1/2} \frac{z_{e_w}\Theta_w^{3/2}}{\lambda_{e_w}}. \quad (36)$$

The quantities V and θ appearing in (29)—(31) must be determined by solving the over-all shock-layer equations. These equations have been obtained by modifying the equations given by Blottner [12]. The detailed expressions of these equations and the procedure to obtain the solutions are described in [10].

III. Formulation in a Free Stream

Since the electron temperature is generally higher than the heavy-particle temperature in the free stream, the electron temperature decreases toward the shock due to the thermal relaxation, but near the shock it increases due to the thermal-layer effect. This was analyzed by Grewal and Talbot [1] for a normal shock in partially ionized argon. The thermal layer of the electrons is caused by the large thermal-conductivity of the electrons. Then it is necessary to solve the electron-energy equation including a thermal-conduction term to determine an electron-temperature profile in the free stream. The net production rates of the electron density and population density are dependent on the electron temperature so that the change in the electron temperature causes those in the electron density and population density. Hence the continuity equations of the electrons and excited atoms must be solved. In the free-stream condition considered here, the relaxation time of any level above 4s ($j=2$) is much shorter than the characteristic flow time so that steady-state populations may be assumed for such levels. On the other hand, the relaxation time of level 4s amounts to only a tenth of the characteristic flow time. Therefore we must solve the continuity equation of the atoms in this level. Since the relaxation time of ionization-recombination is much larger than the characteristic flow time, the ionization-recombination may be taken to be frozen. This leads to constant electron density in the free stream. Any other quantities are not dependent on the electron temperature, and hence they are constant. Ultimately it follows that the equations to be solved in the free stream are the continuity equation of the excited atoms in level 4s and the electron-energy equation.

If the present analysis is restricted to the stagnation stream line, the detached bow-shock may be regarded as a normal shock, as shown in Fig. 3, where the flow is taken to be one-dimensional. The one-dimensional, inviscid electron-energy equation is given by

$$\frac{3}{2}\bar{u}\frac{d}{d\bar{y}}(n_e k_B T_e) = -\frac{5}{2} n_e k_B T_e \frac{d\bar{u}}{d\bar{y}} + \frac{d}{d\bar{y}}\left(\lambda_e \frac{dT_e}{d\bar{y}}\right) + R + L, \quad (37)$$

where $\bar{u}$ is the velocity in the $\bar{y}$-direction. The relation between $\bar{y}$ and y is $\bar{y}+y=y_s$. The terms L and R in (37) are given by (12) and (13), respectively. The following dimensionless quantities are introduced:

$$\Phi = T_a/T_{a\infty}, \quad \Xi = n_e/n_{e\infty} = U_\infty/\bar{u},$$
$$\lambda_e/\lambda_{e_r} = (\Theta/\tilde{\tau})^{5/2}, \quad \tilde{\tau} = T_{e_r}/T_{a\infty}, \quad (38)$$

where the subscript r denotes the condition at a reference point in the free stream. In the present analysis, the reference point is taken at $y/y_s=10$, i.e. at a distance from the wall ten times the shock layer thickness. Using a coordinate transformation $\zeta = (3/2)(\tilde{\tau}^{5/2} n_{e\infty} U_\infty k_B/\lambda_{e_r})\bar{y}$ and the dimensionless quantities given by (38), (37) is transformed to

$$\frac{d}{d\zeta}\left(\Theta^{5/2}\frac{d\Theta}{d\zeta}\right) - \frac{d\Theta}{d\zeta} + \frac{2}{3}\frac{\Theta}{\Xi}\frac{d\Xi}{d\zeta} + \frac{R+L}{a} = 0 \quad (39)$$

with

$$a = (9/4)(k_B^2 \tilde{\tau}^{5/2} n_{e\infty}^2 U_\infty^2 T_{a\infty}/\lambda_{e_r}). \quad (40)$$

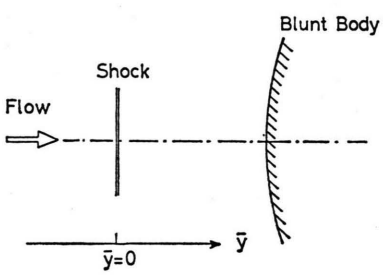

Fig. 3. Shock Model near Stagnation Streamline.

The parameter a denotes the characteristic transfer rate of the electron energy due to thermal conduction. In the free stream, $n_e = \text{const}$ and hence $\Xi = \text{const}$ so that we have

$$\frac{\mathrm{d}}{\mathrm{d}\zeta}\left(\Theta^{5/2}\frac{\mathrm{d}\Theta}{\mathrm{d}\zeta}\right) - \frac{\mathrm{d}\Theta}{\mathrm{d}\zeta} + \frac{R+L}{a} = 0. \quad (41)$$

The boundary condition is

$$\Theta = \tilde{\tau} \quad \text{at} \quad \zeta = \zeta_r. \quad (42)$$

The reference point ζ_r corresponds to $y/y_s = 10$. Another boundary condition is given at the shock position. Integrating (39) from $\zeta = -0$ to $\zeta = +0$, we have

$$\left[\Theta^{5/2}\frac{\mathrm{d}\Theta}{\mathrm{d}\eta}\right]_{+0} - \left[\Theta^{5/2}\frac{\mathrm{d}\Theta}{\mathrm{d}\eta}\right]_{-0} - \Theta_{+0} + \Theta_{-0} + \frac{2}{3}\int_{-0}^{+0}\Theta\frac{\mathrm{d}}{\mathrm{d}\zeta}\ln\Xi\,\mathrm{d}\zeta + \frac{1}{a}\int_{-0}^{+0}(R+L)\,\mathrm{d}\zeta = 0, \quad (43)$$

where $\zeta = -0$ denotes the position immediately ahead of the shock and $\zeta = +0$ is the position immediately behind the shock. The thermal-layer thickness of the electrons is much larger than the thickness of the atom shock, so that the electron temperature does not vary across the shock [1, 3], and hence $\Theta_{+0} = \Theta_{-0} = \Theta_0 = \text{const}$. Introducing a new variable $Y = \Theta^{5/2}\mathrm{d}\Theta/\mathrm{d}\zeta$, (43) is rewritten as

$$Y_{+0} - Y_{-0} + (2/3)\Theta_0 \cdot \ln[1 + 3(M_\infty^2 - 1)/(M_\infty^2 + 3)] = 0, \quad (44)$$

where M_∞ is the free-stream Mach number. In the derivation of (44) we have considered that the electron density obeys the Rankine-Hugoniot relation across the shock. (44) represents the discontinuity of the electron temperature gradient across the shock and also is another boundary condition for (41). The free-stream solution of the electron temperature is connected with the shock-layer solution by means of (44), and the shock-layer solution must satisfy the wall condition given by (36). Therefore, the gradient of the electron temperature must be determined in such a way that the shock layer solution of the electrons satisfies the boundary condition given by (36).

In addition to the electron energy equation, the continuity equation of the atoms in level 4s ($j = 2$) is required to complete the free-stream equations. This is expressed in dimensionless form as

$$\mathrm{d}\bar{\alpha}_2/\mathrm{d}\zeta = \tau_f \dot{n}(2)/n_\infty \quad (45)$$

with

$$\tau_f = \frac{\lambda_{e_r}}{(3/2)\,k_B\,\tilde{\tau}^{5/2}\,n_{e\infty}\,U_\infty^2}, \quad \bar{\alpha}_2 = \frac{n(2)}{n_\infty}. \quad (46)$$

The boundary condition for $\bar{\alpha}_2$ is

$$\bar{\alpha}_2 = \bar{\alpha}_{2_r} \quad \text{at} \quad \zeta = \zeta_r. \quad (47)$$

The quantity $\bar{\alpha}_{2_r}$ must be given as the initial condition.

IV. Transition Rate Constants

In the present work, Drawin's expression for the electronical-excitation rate constants [13] was employed which, for optically-allowed transitions, is

$$Q(j,k) = 4\pi a_0^2 K_{j,k} f_{j,k}\bar{v}\left(\frac{R_\infty}{k_B T_e}\right)^2 \frac{\exp(-u_{j,k})}{u_{j,k}(u_{j,k}+1)} \cdot\left\{\frac{1}{20+u_{j,k}} + \ln[1.25\,\delta_{j,k}(1+1/u_{j,k})]\right\}, \quad (48)$$

and for parity-forbidden transitions, is

$$Q(j,k) = 4\pi a_0^2 K_{j,k}\bar{v}\,u_{j,k} \cdot\left[\frac{\exp(-u_{j,k})}{u_{j,k}} - \int_{u_{j,k}}^{\infty}\frac{\exp(-x)}{x}\mathrm{d}x\right], \quad (49)$$

where a_0 is the first Bohr radius, R_∞ the Rydberg constant, $\bar{v}$ the mean velocity expressed as $(8k_B T_e/\pi m_e)^{1/2}$, $f_{j,k}$ the absorption oscillator strength, $K_{j,k}$ and $\delta_{j,k}$ are parameters, and $u_{j,k} = |E_j - E_k|/k_B T_e$. The parameter $\delta_{j,k}$ is assumed to be unity for all transitions except the 3p—4s transition and is taken to be 0.8 for the 3p—4s transition [14]. The parameter $K_{j,k}$ was estimated from the cross-section expressions of electronical excitation, which were determined with the multipole expansion method proposed by Sobelman [15]. The values of $K_{j,k}$ are summarized in [16].

For ionizations, also Drawin's expression was used. It is written as

$$Q_I(j,\infty) = 4\pi a_0^2\bar{v}\left(\frac{R_\infty}{k_B T_e}\right)^2 \frac{\exp(-u_{j,\infty})}{u_{j,\infty}(u_{j,\infty}+1)} \cdot\left\{\frac{1}{20+u_{j,\infty}} + \ln\left[1.25\left(1+\frac{1}{u_{j,\infty}}\right)\right]\right\}, \quad (50)$$

where $u_{j,\infty} = (E_I - E_j)/k_B T_e$.

The radiative transition probabilities (Einstein A coefficients) between bound excited-levels were calculated from of the wave function given by Bates

and Damgaard [17]. As a first approximation, radiations terminated in any level except for the ground level are taken to be optically thin, which leads to the radiative-escape factor to be unity.

V. Method of Calculation

It is very easy to find the solutions if the solving of the electron-energy equation is considered on the Θ-Y plane. In Fig. 4, the method of solving the electron energy equation is shown for $\Theta_r = 8$ and $[n(2)]_r = 10^{17}$ particles/m^3. At $\zeta = \zeta_r$ corresponding to $y/y_s = 10$ in the free stream, $\Theta_r = 8$ and $[n(2)]_r = 10^{17}$ particles/m^3 are given. For an arbitrarily given value of $d\Theta/d\zeta$ at $\zeta = \zeta_r$, the electron-energy equation (41), coupled with (45), is numerically integrated from the reference point $\zeta = \zeta_r$ corresponding to $y/y_s = 10$ to the shock position corresponding to $y/y_s = 1$. The solution of the electron temperature obtained in this way is illustrated by the curve Γ_1 on the $\Theta - Y$ plane, and the positions r and 1 denote the reference point and the position immediately ahead of the shock, respectively. The position 1 provides the values of Θ and Y at $\zeta = -0$ and hence Θ_0 and Y_{-0}, so that by employing these values in (44), the value of Y_{+0} can be easily obtained. The curve Γ_2 is given by (44), and the position s denotes the condition immediately behind the shock. The value of α_2 immediately behind the shock is equal to that immediately ahead of the shock, and we also have $\alpha_{e_s} = \alpha_{e\infty}$. The condition immediately behind the shock is identical to that at the shock layer edge. The next procedure is to analyze the shock layer. Once the conditions at the shock layer edge are determined, one can start integrating (29)—(31) at the shock layer edge, using an iteration method. By taking $\Theta = \Theta_0$ and $z_2 = 1$ in the shock layer, (30) is numerically integrated in such a way that z_e satisfies the boundary condition given (35). Using this solution in (31), this equation can be integrated, starting at the shock layer edge while z_2 is kept constant yet. (29) is numerically solved by using the solutions of z_e and Θ. The next step is to renew the solution of z_e by using the solutions of Θ and z_2 in (30). Thus, valid solutions of Θ, z_e and z_2 are determined by means of the iteration scheme. The solution of Θ in the shock layer is shown by the curve Γ_3; the point w denotes the wall condition. It is unknown at this stage yet whether the thus determined Θ_w satisfies the boundary condition on the wall, Equation (36). In the same way as described above, one must try to integrate (41) for different values of $(d\Theta/d\zeta)_r$, starting at the reference position, and then to integrate (31). Thus, one can obtain Θ_w and Y_w for different values of $(d\Theta/d\zeta)_r$. The curve Γ_4 expresses the locus of Y_w obtained for the different values of $(d\Theta/d\zeta)_r$. The curve Γ_5 shows the relationship of Θ_w and Y_w calculated by the boundary condition on the wall, Equation (36). Since the reasonable solution of Θ must exist on both of the curves Γ_4 and Γ_5, the intersection of these curves will give the valid condition on the wall. Therefore, the solution of the electron temperature is shown by the curve r-1-s-w. At each stage of the calculation, (1) must be coupled with the electron continuity equation, the continuity equation of excited atoms in level 4s and the electron energy equation to determine the population densities of levels above 4s.

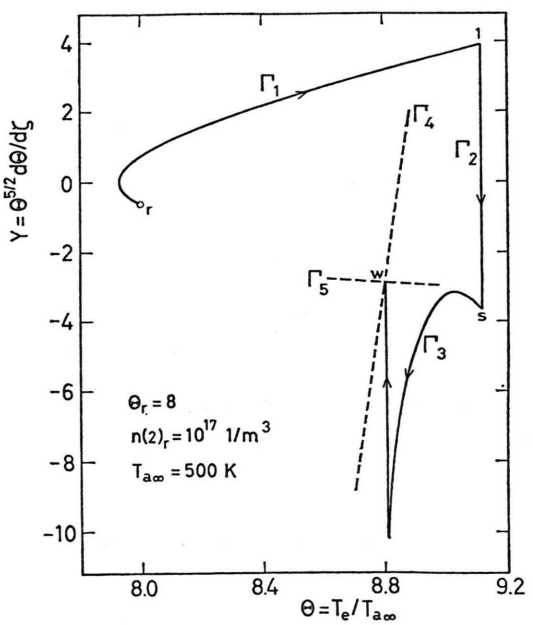

Fig. 4. Method of Solving the Electron Energy Equation.

VI. Calculated Results and Discussions

The calculations were carried out for the following conditions:

$$M_\infty = 4.5, \quad R_N = 4 \times 10^{-2}\ \text{m},$$
$$T_{a\infty} = 500\ \text{K}, \quad n_\infty = 10^{21}\ \text{particles/m}^3,$$
$$n_{e\infty} = 5 \times 10^{19}\ \text{particles/m}^3,$$
$$T_w = 300\ \text{K}, \quad Re_s = 28.9,$$

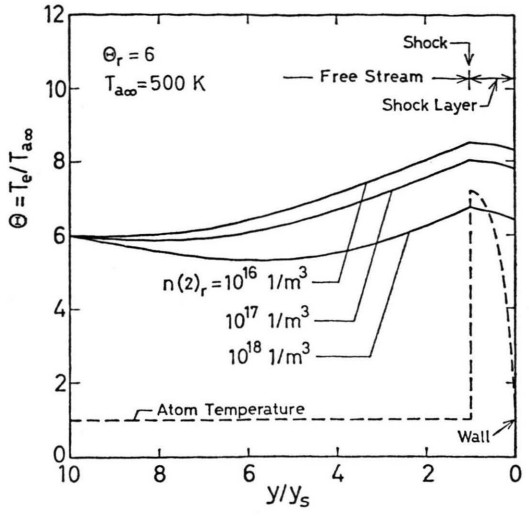

Fig. 5. Electron Temperature Distribution from a Free Stream to a Wall for $\Theta_r = 6$.

where $Re_s = \rho_\infty U_\infty R_N/\mu_s$, T_w is the wall temperature. The above conditions are typical for an arc-heated, low-density plasma flow.

In Fig. 5 are shown the electron temperature distributions from the reference point in the free stream ($y/y_s = 10$) to the body wall ($y/y_s = 0$), for the three cases $[n(2)]_r = 10^{16}$, 10^{17} and 10^{18} particles/m^3. For each case, $\Theta_r = 6$ is taken. The atom-temperature distribution is also illustrated in this figure. In the case of $[n(2)]_r = 10^{18}$ particles/m^3, the electron temperature decreases toward the shock, in the upstream region, and then it increases. The calculated results show that, in the region of the reduction in the electron temperature, the electron gas releases its energy due to inelastic collisions which cause collisional excitation as a net transition. In this region, the electron temperature is higher than the atom temperature, so that the electrons lose their energy due to elastic collisions to equilibrate the temperatures of the electrons and atoms. Thus, both the excitations and the thermal relaxation contribute to the reduction in the electron temperature. The following elevation in the electron temperature is caused by thermal conduction. The electron temperature at any position increases with decreasing $[n(2)]_r$. When $[n(2)]_r$ is small, the contribution of the excitations becomes small, which leads to a small loss of the electron energy. In fact, when $[n(2)]_r = 10^{18}$ particles/m^3, L/R varies from 0.24 at $y/y_s = 10$ to 0.43 at $y/y_s = 1$, while, for $[n(2)]_r = 10^{16}$ particles/m^3, L/R varies 0.096 at $y/y_s = 10$ to 0.048 at $y/y_s = 1$. Thus it is obvious that the excitations significantly affect the electron temperature.

The distributions of the population densities of levels 4p ($j = 3$), 3d ($j = 4$), 5s ($j = 5$), 5p ($j = 6$), 6p ($j = 10$) and 8d ($j = 21$) are shown for the three cases of $[n(2)]_r = 10^{18}$, 10^{17} and 10^{16} particles/m^3 in Figs. 6 to 8, where the population densities are divided by the statistical weight $g(j)$ of a level j. In these figures, the population densities of level 4s ($j = 2$) are not shown because the radiation originating from this level is ultraviolet, so that this radiation may be excluded from the discussion of the dark space. The population density of level 8d is illustrated in the figure in order to show the equilibrium population density. The result for the case of $[n(2)]_r = 10^{18}$ particles/m^3 is shown in Fig. 6, where, in the free stream, the population density of level 8d increases and then decreases toward the shock. The region of the increase in the population density of this level corresponds to the decrease in the electron temperature shown in Figure 5. This is because the equilibrium population density given

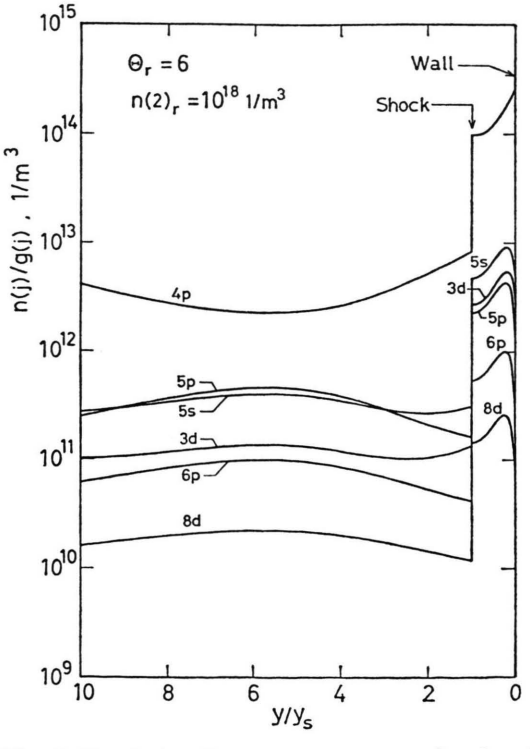

Fig. 6. Population Density Distributions for $\Theta_r = 6$ and $[n(2)]_r = 10^{18}$ particles/m^3.

by the Saha equilibrium relation increases with decreasing electron temperature. The following decrease in the population density of level 8d is also caused by the elevation in the electron temperature. The distributions of the population densities of levels 5p and 6p are very similar to that of level 8d. In particular, the radiation originating from level 5p is in the visible range, so that the reduction in the population density of this level ahead of the shock gives an explanation for the dark space. Thus, the region of elevated electron temperature ahead of the shock corresponds to a region of reduced population density, namely a region of *reduced radiation-emitting atom density*. The results for levels 3d and 5s also illustrate an effect similar to that for level 8d. However, the population densities of these levels increase ahead of the shock. The result for level 4p shows the reduced population density in the region of the decrease in the electron temperature. The reduction in this population density is due to the de-excitation 4p→4s, and the following elevation is caused by the excitation 4s→4p. These excitations and de-excitations are predominant over those between level 4p and upper levels. Ahead of the shock, excitations from level 4p to level 3d and 5s slightly contribute to the elevation in the population densities of levels 3d and 5s. Therefore, not only for the radiations originating from level 4p but also for those originating from levels 3d and 5s, no dark space is observed for the present conditions. The result for $[n(2)]_r = 10^{17}$ particles/m³ shown in Fig. 7 is similar to those in Figure 6.

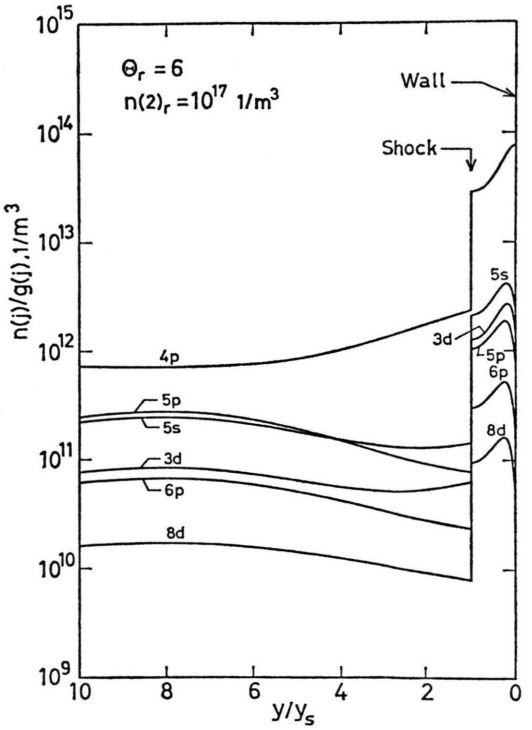

Fig. 7. Population Density Distributions for $\Theta_r = 6$ and $[n(2)]_r = 10^{17}$ particles/m³.

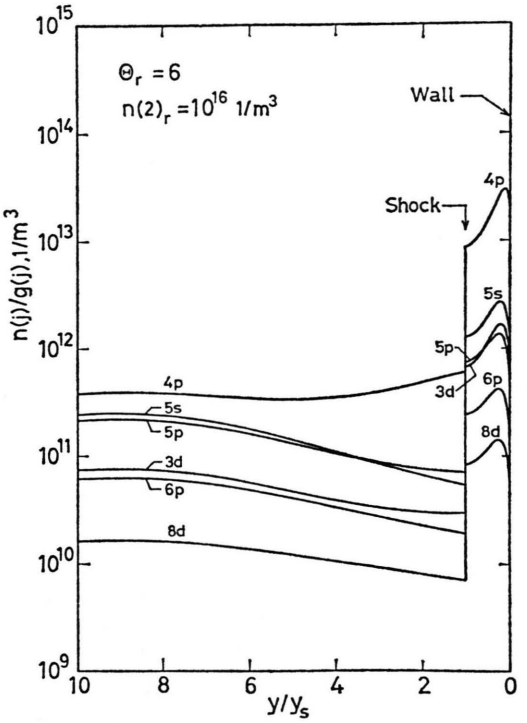

Fig. 8. Population Density Distributions for $\Theta_r = 6$ and $[n(2)]_r = 10^{16}$ particles/m³.

Figure 8 depicts the results for $[n(2)]_r = 10^{16}$ particles/m³. We can observe that ahead of the shock, the population densities of levels higher than level 3d decrease as the electron temperature increases. On the other hand, the result of level 4p shows an elevation in the population density of this level. This is because the population density of this level is also supplied by the excitation 4s→4p. Although the excitations 4p→3d and 4p→5s slightly influence the population densities of levels 3d and 5s, the population densities of these levels do not increase. Therefore, we may state that the dark space can be observed for the radiations originating from levels higher than 3d, but that the radiation originating from level 4p produces no dark space.

The electron-temperature distribution for $\Theta_r = 6$ is compared with that for $\Theta_r = 8$ in Fig. 9, where, for both cases, $[n(2)]_r$ is kept to be 10^{17} particles/m^3. The feature of the electron-temperature variation for $\Theta_r = 8$ is very similar to that for $\Theta_r = 6$. Figure 10 illustrates the population-density distributions for $\Theta_r = 8$. In comparison with the result for $\Theta_r = 6$, the variation is slight. Ahead of the shock, the population densities of levels 4p, 3d and 5s show the slight elevation so that the radiations originating from these levels causes no dark space. On the other hand, the population densities of level 5p is reduced there, which leads to the dark space.

VII. Concluding Remarks

The principal conclusions as to the argon atoms which may be drawn from this investigation are summarized as follows:

1) The population densities of the levels higher than level 5s are reduced ahead of the shock, corresponding to the elevation in the electron temperature. The region of reduced population density can be explained as the so called dark space where the radiation intensity is reduced.

2) The dark space is produced due to the elevation in the electron temperature ahead of the shock. As the electron temperature increases, the equilibrium population densities of upper levels will be reduced. This reduction propagate down to lower levels through electron-collisional de-excitations. Thus, the reduction in the population density causes the dark space, so that the dark space can be observed only in radiations originating from electronically excited levels, and it is not observed in radiations originating from *rotationally-vibrationally excited levels.*

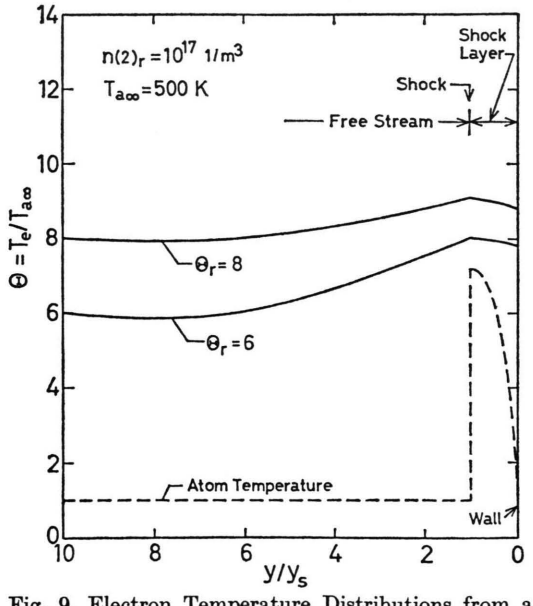

Fig. 9. Electron Temperature Distributions from a Free Stream to a Wall for $[n(2)]_r = 10^{17}$ particles/m^3.

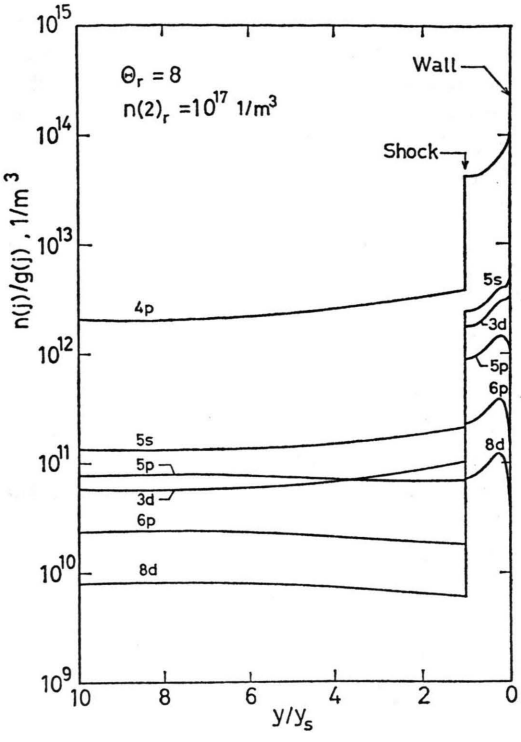

Fig. 10. Population Density Distributions for $\Theta_r = 8$, and $[n(2)]_r = 10^{17}$ particles/m^3.

3) The population density of level 4p is elevated ahead of the shock so that no dark space can be observed in the radiation originating from this level.

4) When the population density of level 4s at the reference point in the free stream is large, or when the electron temperature in the free stream is high, the population densities of levels 3d and 5s are elevated ahead of the shock.

5) When the population density of level 4s at the reference point is 10^{18} particles/m^3, the ratio of the electron-energy transfer rates due to inelastic and elastic collisions varies from 0.24 to 0.43 in the free stream, so that in this condition the influence of the inelastic collisions on the electron temperature is significant.

[1] M. S. Grewal and L. Talbot, J. Fluid Mech. **16**, 573 (1963).
[2] W. H. Christiansen, Phys. Fluids **10**, 2586 (1967).
[3] M. Y. Jaffrin, Phys. Fluids **8**, 606 (1965).
[4] "Population density" is employed in place of "number density of excited atoms".
[5] M. Mitchner and C. H. Kruger, Partially Ionized Gases, John Wiley & Sons, New York 1973.
[6] C. H. Kruger and M. Mitchner, Phys. Fluids **10**, 1953 (1967).
[7] G. W. Sutton and A. Sherman, Engineering Magnetohydrodynamics, McGraw-Hill, New York 1965, Chapter 4.
[8] W. S. Liu, B. T. Whitten, and I. I. Glass, J. Fluid Mech. **87**, 609 (1978).
[9] M. Nishida, The Memoirs of the Faculty of Engineering, Kyoto University, XLII, 265 (1981).
[10] M. Nishida, Phys. Fluids **15**, 596 (1972).
[11] S. P. Knöös, J. Plasma Phys. **2**, 207 (1968).
[12] F. G. Blottner, AIAA J. **7**, 2281 (1961).
[13] H. W. Drawin, EUR-CEA-FC-383, Association Euratom-C.E.A., Fontenay-aux-Roses, France 1967.
[14] K. Katsonis, EUR-CEA-FC-820, Association Euratom C.E.A., Fontenay-aux-Roses, France 1976.
[15] I. I. Sobelman, Introduction to the Theory of Atomic Spectra, Pergamon Press, Oxford 1972, Chapter 11.
[16] A. Kimura, M. Nishida, and P. Valentin, J. Physique, to be published.
[17] D. R. Bates and A. Damgaard, Phil. Trans. Soc. London **A 242**, 101 (1950).